Two-nucleon absorption of stopped π^- in ^{3}He

Jacob Roginsky and Carl Werntz
Physics Department, The Catholic University of America, Washington, D.C. 20064
(Received 7 October 1988; revised manuscript received 3 April 1989)

A phenomenological two-nucleon pion-absorption T matrix is used to calculate partial rates for absorption of negative pions from the 1s state of the ^{3}He pionic atom. The T matrix depends on parameters g_0 and g_1, which describe absorption on s-wave triplet and singlet nucleon pairs, respectively. The partial rates considered are those feeding $n+d$, $n+{}^1(np)_0$, $p+{}^1(nn)_0$, and those nnp final states with no nucleon pairs of low relative energy. In addition, the differential rate to the nnp final state is calculated as a function of T_n and T_p, observed neutron and proton kinetic energies, respectively, and is compared to experimental differential rates along selected straight lines in a Dalitz plot of event number density vs T_n and T_p. Two different momentum space ground-state functions are used, both exhibiting the correct asymptotic behavior with respect to bound two-body and three-body channels but derived from wave functions in configuration space with and without hard-core nucleon-nucleon correlations. Agreement with a number of recent pion absorption experiments can only be obtained with the wave function containing hard-core correlations and only for small positive values of g_1/g_0, $g_1^2/g_0^2<0.04$, much smaller than the ratio $g_1^2/g_0^2=0.30\pm0.15$, which is consistent with the low-energy production cross sections for $p+p\rightarrow d+\pi^+$ and $p+p\rightarrow p+p+\pi^0$. It is suggested that the discrepancy arises because gamma rays from pp bremsstrahlung may have contributed significantly to the measured π^0 production cross sections and/or because single nucleon processes may play a significant role in low-energy absorption on singlet nucleon pairs.

I. INTRODUCTION

The ^{3}He nucleus is the simplest nucleus with more than two nucleons that can be used as a target for pions in order to study the two-nucleon model of pion absorption. Only two distinct particle channels, nnp and nd, can be reached by absorption of π^- so that kinematically complete experiments are feasible. Its mirror nucleus, ^{3}H, can also be used in experiments, so that the isospin properties of the absorption operator can be studied. The ^{3}He nucleus is convenient for theoretical pion-absorption studies as well, since both initial- and final-state three-body wave functions are available.

Ashery and Schiffer[1] have written a review article on pion absorption in which they distinguish experiments and theory dealing with pions of low energy and those concerned with higher energy, where formation of the (3,3) resonance is the dominating mechanism. To a large extent absorption of pions in ^{3}He pionic atoms occurs when pions in orbital s states are absorbed on nucleon-nucleon pairs in relative s states, so the (3,3) resonance is unimportant. The isolation of s-wave absorption from p-wave absorption makes the study of absorption in ^{3}He pionic atoms very attractive.

Following Brueckner's suggestion[2] that pion absorption in nuclei occurs on deuteron pairs, Eckstein[3] introduced a phenomenological zero-range two-nucleon operator which provided for absorption of pions on spin-singlet nucleon pairs in ^{4}He as well as triplet spin pairs. The parameters for the operator were obtained from an analysis of threshold nucleon-nucleon pion production cross sections for $p+p\rightarrow d+\pi^+$ and $p+p\rightarrow p+p+\pi^0$. Several other authors[4–6] made refinements and extensions of this model and applied it to ^{3}He. In general, these calculations used (1) zero-range pair interactions, (2) square well or Hulthen deuteron wave functions, and (3) completely phenomenological Gaussian or Gunn-Irving three-body bound-state wave functions with no strong nucleon-nucleon correlations. The calculated quantities were, typically, the total absorption rates to the nd and nnp final states and the momentum spectrum of protons in the latter channel.

The calculations of Phillips and Roig[7] represented significant progress toward more realistic models. Carrying out the calculations in momentum space, they used two- and three-body bound-state wave functions with correct asymptotic behavior and consistent short-range correlations. They also examined effective Hamiltonians for two-nucleon absorption with the zero-range delta function $\delta^3(\mathbf{r}_1-\mathbf{r}_2)$ replaced by finite-range (albeit still short range, $a=0.6$ fm) form factors of a variety of functional shapes. At the time of their work there was essentially one experiment with which to compare theoretical results, that of Zaimidoraga *et al.*[8] in which the relative yields of nd, nnp, and $^3\mathrm{H}\gamma$ from π^- stopped in a ^{3}He gas target were measured.

More recently, the results from a number of stopped pion ^{3}He experiments have been published that afford the opportunity for a more definitive study of the two-nucleon absorption model. The new experiments include (1) direct measurements of the total ^{3}He 1s width,[9,10] (2) additional measurements of the relative sizes of partial rates,[11–15] (3) kinematically complete measurements[13] of the nnp final state, and (4) relative and absolute partial

rates from the 1*s* orbit leading to *nd*, *nnp*, and $^3H\pi^0$ channels (and $^3H\gamma$ by subtraction). The experiment that originally motivated this paper was a kinematically complete one,[13] in which each measured three-nucleon final-state event was registered as a point on a Dalitz plot. The axes of this plot are the kinetic energies of the proton and a neutron, T_p and T_n, respectively. The allowed kinematic region can be divided into sectors attributable to quasi-free absorption (QFA) on either *pp* or *np* pairs and sectors mostly associated with final-state interactions (FSI's). The latter are characterized by the emission of pairs of nucleons with low relative momentum. They are analogues of the two-body *nd* channel, whose branching ratio was also measured following absorption of stopped pions. The data is summarized in Table I, which is a reproduction of Table I of Ref. 13 altered by us to reflect corrected neutron efficiencies reported[15] by the same experimental group. The effect of the correction is to raise the *nd* branching ratio and to lower the three-nucleon ratios.

An examination of the theoretical rates of Phillips and Roig[7] reveals that they can be brought into agreement with the newer three-body experiments by allowing the parameter g_1, which fixes the strength of absorption on singlet spin nucleon-nucleon pairs, to vary from its value derived for $p+p\to p+p+\pi^0$, while keeping the value of g_0, which is derived from the significantly more accurate experiment $p+p\to d+\pi^+$, fixed. This circumstance encouraged us to repeat the calculations of Ref. 7 and to augment them by (1) calculating the partial rates for absorption leading to the FSI channels $n\,^1(np)_0$ and $p\,^1(nn)_0$, treated on the same footing as the *nd*, (2) calculating differential partial rates as functions of T_n and T_p for comparison to the Dalitz plot of Ref. 13, and (3) examining the effect of much larger form-factor ranges, $0.6\le a\le 1.8$ fm, on the partial rates.

TABLE I. Branching ratio (in percent) for post-absorption final states of stopped π^- in ^{3}He. This table is a reproduction of Table I, Ref. 13 with the *nd* rate increased following Ref. 15, and the three-body rates decreased accordingly.

nnp	QFA ($np\to nn$)	64.8±10.0
channel	QFA ($pp\to np$)	5.9±0.4
	FSI *nn*	1.5±0.4
	FSI *np*	11.7±1.7
nd channel		16.1±2.5
		100

II. SUMMARY OF THE THEORY

A. Two-nucleon pion-absorption *t* matrix

In the two-nucleon model for *S*-wave pion absorption, a pion scatters from one nucleon then propagates off shell to the second nucleon, where it is absorbed.[16–18] Using the notation of Phillips and Roig,[7] this process can be modeled by a phenomenological *t* matrix for low-energy π^+ production

$$\langle \mathbf{k},\mathbf{p}|t|\mathbf{p}'\rangle=\frac{1}{2(2\pi)^{9/2}}f(\mathbf{p}'-\mathbf{p})[g_0(\sigma_1+\sigma_2)(\tau_1^-+\tau_2^-)+g_1(\sigma_1-\sigma_2)(\tau_1^-+\tau_2^-)]\cdot(\mathbf{p}'-\mathbf{p})\ , \tag{1}$$

where $\mathbf{p}'$ is the initial relative momentum of the incoming nucleon pair, $\mathbf{p}$ is the final relative momentum, and $\mathbf{k}$ is the momentum of the pion in the c.m. frame. The intermediate state propagation of the pion is described by the form factor $f(\mathbf{k})$, which in the present work is approximated by two forms, exponential and Yukawa:

$$\begin{aligned}&\text{exponential: } f(\mathbf{k})=(k^2a^2+1)^{-2}\ ,\\ &\text{Yukawa: } f(\mathbf{k})=(k^2a^2+1)^{-1}\ .\end{aligned} \tag{2}$$

For physical reasons, the Yukawa form was used almost exclusively. Because of the large momentum transfer involved in the process, Phillips and Roig[7] used rough uncertainty principle arguments to deduce that $a\simeq(M\mu)^{-1/2}=0.54$ fm. However, the intermediate state pion is "less" off shell than the virtual pion responsible for the long-range part of the nucleon-nucleon force, so $a\simeq\mu^{-1}=1.4$ fm is perhaps more realistic. We have considered values of a in the range 0.6 fm $\le a\le$ 1.8 fm.

The Rosenfeld analysis[19] of the energy dependence of the various pion production cross sections has been reviewed and the parameters updated by Long, Sternheim, and Silbar.[20] For the production of pions in *s* waves relative to the three-body center of mass, the two reactions and their leading energy dependences near threshold are[20]

$$\begin{aligned}&p+p\to d+\pi^+,\quad \sigma=240\eta(\mu b)\ ,\\ &p+p\to p+p+\pi^0,\quad \sigma=27.6\eta^2(\mu b)\ .\end{aligned} \tag{3}$$

In these equations, η is the maximum momentum of the pion in the $NN\pi$ center of mass expressed in units of μ, the pion mass. The value used by Phillips and Roig[7] for the low-energy $d+\pi^+$ parameter was the same, but they used $25\eta^2$ for the $p+p+\pi^0$. They quote errors of ±8% for the first cross section and ±50% for the second. The values for $\sigma(p+p\to p+p+\pi^0)$ differ slightly because the authors of Ref. 20 fitted the experimental data of Dunaitsev and Prokoshkin[21] rather than that of Ref. 22, used by Phillips and Roig. The 50% error in the π^0 production parameter is probably a realistic estimate because of the difficulty in measuring the very small cross section.

The parameters in the *t* matrix, Eq. (1), are fixed by requiring that the low-energy cross sections of Eq. (3) be reproduced. The *T* matrices for the two processes (*s*-state nucleons, *s*-state pion) are

$$\langle \mathbf{k}|T|\mathbf{p}_i\rangle=\int d^3p\langle 00|\langle 1M_f|\Phi_d^*(\mathbf{p})\langle \mathbf{k},\mathbf{p}|t|\mathbf{p}_i\rangle|1M_i\rangle|11\rangle\ , \tag{4a}$$

$$\langle \mathbf{k},\mathbf{p}_f|T|\mathbf{p}_i\rangle = \int d^3p \langle 11|\langle 00|\Phi^-_{p_f}(\mathbf{p})^*\langle \mathbf{k},\mathbf{p}|t|\mathbf{p}_i\rangle|1M_i\rangle|11\rangle \ , \tag{4b}$$

where the spin-isospin functions for the initial and final two-nucleon states have been introduced. The $d\pi^+$ production amplitude, Eq. (4a), is proportional to g_0, the $pp\pi^0$ amplitude and Eq. (4b) to g_1. Invoking charge independence, the pp final state is treated like the np. Phillips and Roig[7] considered Hulthen, soft-core and hard-core two-nucleon correlations. In the present work only the two extreme cases are considered, and the Hulthen result is derived from the hard core by letting the hard-core radius $r_c \to 0$. While our calculations are carried out in momentum space, the model wave functions for the deuteron and singlet pp states are more simply expressed in configuration space. In this space the two wave functions are

$$\Phi_d(\mathbf{r}) = N_d^{1/2}\frac{e^{-\alpha_d(r-r_c)}}{r}(1-e^{-\beta_d(r-r_c)}), \quad r \geq r_c, \ \alpha_d^2 = M\varepsilon_b \ ,$$
$$= 0, \quad r \leq r_c \ , \tag{5a}$$

where M is the nucleon mass, ε_d, the deuteron binding energy, and

$$\Phi^-_{p_f}(\mathbf{r}) = \frac{e^{-i\delta}}{(2\pi)^{3/2}p_f r}[\sin(p_f r+\delta) - \sin(p_f r_c+\delta)e^{-\beta_s(r-r_c)}], \quad r \geq r_c \ ,$$
$$= 0, \quad r \leq r_c \ , \tag{5b}$$

where $\delta(p_f)$ is the $^1S_0$ nucleon-nucleon phase shift. The parameters β_d and β_s are fixed by the requirement that in the zero-energy limit the wave functions yield the correct triplet and singlet effective ranges. The second function, that of an uncharged s-wave NN pair, was not given explicitly in Ref. 7, but it satisfies the correct boundary conditions at $r = r_c$ and for large r. In the limit of $p_f \to 0$ and the singlet scattering length $a_s \to \infty$, it assumes the form of a zero-energy bound state, that is, the same form as the right-hand side (RHS) of Eq. (5a) with $\alpha_d \to 0$. The values of β_d and β_s were taken from Table I, Ref. 7, for the $r_c = 0$ and $r_c = 0.5$ fm cases. The phase shift $\delta(p_f)$ in Eq. (5b) was evaluated from the effective range expansion for singlet np scattering with the parameters taken from Noyes.[23]

The parameters g_0 and g_1 of the production t matrix are given in Table II as functions of the length a, which is essentially the range of the intermediate pion state. The underlined values reproduce within 1% the values for corresponding cases given in Tables 2 and 3 of Phillips and Roig.[7] The other parameter sets were not treated by these authors. Note, that for all tabulated values of a, the ratio $g_1^2/g_0^2 \simeq \frac{1}{4}$ for the $r_c = 0$ functions, and $g_1^2/g_0^2 \simeq \frac{1}{3}$ for $r_c = 0.5$ fm.

B. Pion absorption from the 1s state

All rates depend on the square of the T matrix for a transition from an initial nuclear ground state Ψ_i and pion bound state Φ_i to a final nuclear state Ψ_f. Since the two-body t matrix is in momentum space and has no explicit dependence on the pion momentum,

TABLE II. Parameters g_0 and g_1 in the phenomenological two-nucleon t matrix of Eq. (1) that fit the low-energy pion production cross sections. The range of the intermediate pion for both the exponential and the Yukawa form factors is allowed to vary between 0.6 and 1.8 fm. Two types of nucleon-nucleon correlations were used in the final-state deuteron and singlet pp wave functions, hard core and Hulthen ($r_c \to 0$). The underlined entries agree with values of Ref. 7.

Range (fm)	Form factor	Hard-core deuteron and singlet deuteron functions		Hulthen deuteron and singlet deuteron functions	
		g_0^2 (fm^8)	g_1^2 (fm^8)	g_0^2 (fm^8)	g_1^2 (fm^8)
0.6	Exponential	<u>33.06</u>	<u>11.74</u>	<u>9.17</u>	<u>2.35</u>
0.6	Yukawa	16.90	5.23	<u>1.73</u>	0.46
1.0	Exponential	304.0	137.8	93.5	25.40
1.0	Yukawa	46.30	14.90	6.67	1.73
1.4	Exponential	1921	1145	560.6	162.6
1.4	Yukawa	120.4	40.7	19.14	4.97
1.8	Exponential	8657	6802	2330	711.0
1.8	Yukawa	271.0	95.6	44.7	11.70

$$T_{fi}=\int d^3k\,\langle\Psi_f|\sum_{\text{all pairs}} t|\Psi_i,\mathbf{k}\rangle\Phi_i(\mathbf{k})$$
$$=\frac{\pi}{\sqrt{\mu}}\Phi_{1s}(0)\langle\Psi_f|t|\Psi_i,0\rangle\ ,$$
$$\Phi_{1s}(0)=2(Z/a_0)^{3/2}R_{1s}(0)\ , \tag{6}$$

where a_0 is the Bohr radius of the pion, Z is the nuclear charge, and $R_{1s}(0)$ is the ratio of the pion wave function at the origin, including strong interaction, to the pion Coulombic wave function. The S-state attraction in ^{3}He (Refs. 9 and 10) implies (Ref. 24) $R_{1s}^2(0)=1.05$. The normalization $\int d^3k|\Phi(\mathbf{k})|^2=(2\mu)^{-1}$ has been adopted in conformity with $\langle\mathbf{k}'|\mathbf{k}\rangle=2\varepsilon_\pi\delta(\mathbf{k}'-\mathbf{k})$, the normalization of the pion momentum states.

C. ^{3}He ground state

In all wave functions standard three-body notation is used. Momenta are designated by $\mathbf{p}_\alpha$ and $\mathbf{q}_\alpha$, which refer to the relative momentum of the particle pair $\beta\gamma$ ($\alpha\beta\gamma$ cyclic permutation of 1,2,3) and to the relative momentum of the particle α and the subsystem $\beta\gamma$, respectively, S_α and T_α refer to the spin and isospin of a single nucleon, and $S_{\beta\gamma}$ and $T_{\beta\gamma}$ denote the coupled spins and isospins of the $\beta\gamma$ pair. The model ground state used in this calculation is one that (1) has the correct asymptotic limits with respect to two-body and three-body channels, (2) contains specific nucleon-nucleon correlation, and (3) has an approximately correct rms radius as deduced from electron scattering. The form introduced by Barbour and Phillips[25] and used in Ref. 7, where only the completely space symmetric S state is retained, is

$$\Psi_i=u(\mathbf{p},\mathbf{q})\frac{1}{\sqrt{2}}(|S_{12}=0,S_3,\tfrac{1}{2}+m_i\rangle|T_{12}=1,T_3,\tfrac{1}{2}+\tfrac{1}{2}\rangle-|S_{12}=1,S_3,\tfrac{1}{2}+m_i\rangle|T_{12}=0,T_3,\tfrac{1}{2}+\tfrac{1}{2}\rangle)\ , \tag{7a}$$
$$u(\mathbf{p},\mathbf{q})=\frac{1}{\sqrt{2}}\sum_{\alpha=1}^{3}\left[\frac{N_d(\mathbf{p}_\alpha,\mathbf{q}_\alpha)}{[q_\alpha^2+\frac{4}{3}M(\varepsilon_B-\varepsilon_d)]}-\frac{N_s(\mathbf{p}_\alpha,\mathbf{q}_\alpha)}{[q_\alpha^2+\frac{4}{3}M(\varepsilon_B-\varepsilon_s)]}\right]\Big/(p_\alpha^2+\tfrac{3}{4}q_\alpha^2+M\varepsilon_B)\ . \tag{7b}$$

The two functions $N_n(\mathbf{p}_\alpha,\mathbf{q}_\alpha), n=d,s$ are proportional to the form factors $g_n(p)$, of separable potential approximations to the low-energy two-nucleon T matrices,

$$N_n(\mathbf{p},\mathbf{q})=g_n(p)\frac{h_n}{(q^2+\nu_n^2)}\ . \tag{8}$$

The form factors are obtained from the Fourier transforms (FT) of the two-nucleon bound-state wave functions through the relation

$$\Phi_n(p)\propto g_n(p)/(p^2+\alpha_n^2)\ .$$

The explicit form of g_n is given by Eq. (A1) in the Appendix. The spin-singlet, isospin-triplet system was assumed to have a zero energy bound state so that $\alpha_s=0$. The second factor in Eq. (8) has adjustable parameters for normalization and for fitting the rms charge radius of the ^{3}He system. The parameters h_n and ν_n are given in Table I of Ref. 7, both for the hard core ($r_c=0.5$ fm) and the Hulthen form factor ($r_c=0.0$ fm).

D. Final-state wave functions and partial absorption rates

The final nucleon states distinguished in the stopped pion experiments (see Table I) are (1) the two-body nd, (2) the quasi-two-body FSI states $n\,^1(np)_0$ and $p\,^1(nn)_0$, and (3) nnp states following QFA, where the relative energy of no pair of nucleons is low.

1. Two-body and FSI states

The wave function for the nd (FSI) channel is taken as the product of an S-state bound (scattering) two-nucleon wave function and a delta function representing a noninteracting third particle,

$$\Psi_f=\frac{1}{\sqrt{3}}\sum_{\alpha=1}^{3}\delta_3(\mathbf{q}_\alpha-\mathbf{q}_f)\Phi_n(p_\alpha)|S_{\beta\gamma},S_\alpha=\tfrac{1}{2},S_fm_f\rangle\sum_{T=1/2}^{3/2}(T_{\beta\gamma}t_{\beta\gamma}T_\alpha t_\alpha|T-\tfrac{1}{2})|T_{\beta\gamma},T_\alpha=\tfrac{1}{2},T-\tfrac{1}{2}\rangle\ ,$$
$$\Phi_n(p)\equiv\Phi_d(p),\quad S_{\beta\gamma}=1,\ T_{\beta\gamma}=0\ \text{ for } n+d\ ,$$
$$\Phi_n(p)\equiv\Phi_{pf}^-(p),\quad S_{\beta\gamma}=0,\ T_{\beta\gamma}=1,\ t_{\beta\gamma}=0,\ t_\alpha=-\tfrac{1}{2}\ \text{ for } n+{}^1(np)_0\ , \tag{9}$$
$$\Phi_n(p)\equiv\Phi_{pf}^-(p),\quad S_{\beta\gamma}=0,\ T_{\beta\gamma}=1,\ t_{\beta\gamma}=-1,\ t_\alpha=+\tfrac{1}{2}\ \text{ for } p+{}^1(nn)_0\ ,$$

Again, the bound-state wave function is the FT of the RHS of Eq. (5a), and the scattering wave function is the FT of the RHS of Eq. (5b). Evaluating the T matrix for the two body and FSI states, we get

$$W^{1s}(n+d)=\frac{|\Phi_{1s}|^2}{3(2\pi)^5}\frac{M}{\mu}(g_0^2+3g_1^2+2g_0g_1)q_f|\mathbf{I}_d|^2\ , \tag{10a}$$

where q_f is the relative momentum of the noninteracting neutron with respect to the deuteron,

$$W^{1s}(n+{}^1np_0)=\frac{|\Phi_{1s}|^2}{3\times2^3(\pi)^4}\frac{M}{\mu}g_0^2\int_0^{p_f^{\max}}p_f^2q_f\,dp_f|\mathbf{I}_s|^2\ , \tag{10b}$$

$$W^{1s}(p+{}^1nn_0)=\frac{g_1^2}{2g_0^2}W^{1s}(n+{}^1np_0)\ , \tag{10c}$$

$$\frac{4q_f^2}{3M}+\frac{p_f^2}{M}=K_f\ . \tag{10d}$$

The deuteron result was obtained by Phillips and Roig,[7] while the singlet results are new to this work. The total available kinetic energy in the singlet cases is K_f. The momentum $p_f^{\max}$ represents a qualitative upper limit on the relative neutron-proton momentum such that an event is attributable to the formation of a singlet *np* pair. The value $p_f^{\max}=0.5\ \text{fm}^{-1}$ was used in all cases. For future reference, the sum of the two rates in Eq. (10b) and (10c) is designated as $W^{1s}(nnp\ \text{FSI})$. The integrals are $n=d,s$,

$$\mathbf{I}_n(\mathbf{q}_f)=\int d^3p_1\int d^3q_1\Phi_n^*(|\mathbf{q}_1+\tfrac{1}{2}\mathbf{q}_f|)[f(|\tfrac{1}{2}\mathbf{q}_1+\mathbf{q}_f+\mathbf{p}_1|)+f(|\tfrac{1}{2}\mathbf{q}_1+\mathbf{q}_f-\mathbf{p}_1|)]u(\mathbf{p}_1,\mathbf{q}_1)(\tfrac{1}{2}\mathbf{q}_1+\mathbf{q}_f)\ . \tag{11}$$

The dependence of each of the three rates in Eq. (10) on g_0,g_1 is easily explained. Either of the deuteron and the singlet ${}^1np_0$ pairs can be formed in the final state by a spectator proton interacting with a neutron from the *np* pair on which the pion is absorbed. Both processes thus contain g_0^2, signaling absorption on an ${}^3S_1$ pair. On the other hand, a ${}^1(nn)_0$ pair can be formed only from a spectator neutron interacting with the neutron from the pion absorption on the remaining ${}^1S_0$ *pp* pair so that the corresponding rate is proportional to g_1^2.

The numerical evaluation of integral $\mathbf{I}_s$, containing the continuum wave function $\Phi_s(\mathbf{p})$, proved to be very time consuming. Singularities in the integrand were eliminated by introducing a cutoff radius R in taking the Fourier transform of the RHS of Eq. (5b). The justification for this simplification is that the integrand of the configuration space integral corresponding to Eq. (11) vanishes for large r because of the finite extents of the ^{3}He wave function and the form factor $f(x)$. A cutoff radius R, conjugate to the momentum variable p, can be chosen such that setting $\Phi_{p_f}^-(\mathbf{r})=0$ for $r>R$ changes the integral by an arbitrarily small amount. The calculations for both the deuteron and singlet deuteron were then carried on the same basis with $\Phi(\mathbf{p})$ being the FT of a localized function in both cases [see Eq. (A2) in the Appendix for the form of $\Phi_{p_f}^-(\mathbf{p})$ with the cutoff radius R].

2. *Quasifree absorption states*

The QFA regions of the Dalitz plot, remote from the low-energy nucleon pair FSI regions, were treated by taking a noninteracting final three-nucleon wave function,

$$\begin{aligned}\Psi_f^3&=\Sigma_{T_f}(1-1\tfrac{1}{2}+\tfrac{1}{2}|T_f-\tfrac{1}{2})\Psi_f^3(T_f)\ ,\\ \Psi_f^3(T_f)&=\frac{1}{\sqrt{6}}\sum_{\alpha=1}^{3}[\delta_3(\mathbf{q}_\alpha-\mathbf{q}_f)\delta_3(\mathbf{p}_\alpha-\mathbf{p}_f)-(-1)^{S_{nn}+T_{nn}}\delta_3(\mathbf{q}_\alpha-\mathbf{q}_f)\delta_3(\mathbf{p}_\alpha+\mathbf{p}_f)]\\ &\quad\times|S_{\beta\gamma}=S_{nn},\tfrac{1}{2},S_fm_f\rangle|T_{\beta\gamma}=T_{nn},\tfrac{1}{2},T_f-\tfrac{1}{2}\rangle\ .\end{aligned} \tag{12}$$

Writing the total rate as an integral over the c.m. neutron and proton kinetic energies T_n and T_p, the integrand is proportional to the density of events on the Dalitz plot with T_n and T_p along the axes.

$$\begin{aligned}W^{1s}(nnp\ \text{QFA})=\frac{|\Phi_{1s}(0)|^2}{2(2\pi)^6\mu}(2\pi^2M^3)\int dT_n\int dT_p\{&2g_0^2|\mathbf{K}_3|^2+g_1^2[|\mathbf{K}_1|^2+|\mathbf{K}_2|^2+|\mathbf{K}_3|^2-(\mathbf{K}_1+\mathbf{K}_2)\cdot\mathbf{K}_3+\mathbf{K}_1\cdot\mathbf{K}_2]\\ &-2g_0g_1(\mathbf{K}_1+\mathbf{K}_2)\cdot\mathbf{K}_3\}\ .\end{aligned} \tag{13}$$

The integrals $\mathbf{K}_\alpha(T_p,T_n)$ are given by

$$\mathbf{K}_\alpha(T_p,T_n)=\mathbf{p}_{\alpha f}\int d^3p[f(|\mathbf{p}_{\alpha f}-\mathbf{p}|)+f(|\mathbf{p}_{\alpha f}+\mathbf{p}|)]u(\mathbf{p},\mathbf{q}_{\alpha f})\ . \tag{14}$$

From symmetry considerations we can infer that any term under the integral sign of the RHS of Eq. (13) can be reduced to either K_1^2 or $\mathbf{K}_1\cdot\mathbf{K}_2$ as far as the total *nnp* QFA rate is concerned. Then Eq. (13) reduces to the form given in Ref. 7. However, the calculation of the doubly differential rate for comparison to the Dalitz plot requires that the expanded form of the integrand be used. The functions $\mathbf{K}_\alpha(T_p,T_n)$ depend on the variables $\mathbf{p}_{\alpha f}$, $\mathbf{q}_{\alpha f}$, and $\mathbf{p}_{\alpha f}\cdot\mathbf{q}_{\alpha f}$. If we choose nucleon 3 to be the proton in the final state and nucleon 1 to be the observed neutron, $\mathbf{p}_{3f}$ and $\mathbf{q}_{3f}$ are related to the observables T_p and T_n by

$$q_{3f}^2=2MT_p,\quad p_{3f}^2=M(K_f-3/2T_p)\ , \tag{15a}$$

and

$$\mathbf{q}_{3f}\cdot\mathbf{p}_{3f}=M(K_f-T_p-2T_n)\ .$$

Then $\mathbf{p}_{\alpha f}$ and $\mathbf{q}_{\alpha f}$, $\alpha=1,2$, are linear combinations of the $\mathbf{p}_{3f}$ and $\mathbf{q}_{3f}$, which can be written symbolically as

$$\begin{bmatrix} \mathbf{p}_{\alpha f} \\ \mathbf{q}_{\alpha f} \end{bmatrix} = P_\alpha \begin{bmatrix} \mathbf{p}_f \\ \mathbf{q}_f \end{bmatrix} . \tag{15b}$$

The P_α are 2×2 matrix representatives of the cyclic permutation elements of the S_3 group which carry the "$\alpha=3$" momenta into "$\alpha=1$" and "$\alpha=2$", respectively. $|\mathbf{K}_\alpha|$ is large in that region of the Dalitz plot where the nucleon α is a low-momentum spectator to QFA on the pair $\beta\gamma$. For example, $\mathbf{K}_3$ is large for $T_p\to0$, so it represents π^- absorption on an np pair. Then $\mathbf{K}_1$ and $\mathbf{K}_2$ represent absorption on pp pairs and are large for either $T_n=0$ or $T_n=T_p=\frac{1}{2}K_f$. If one assumes at any QFA peak along the perimeter of the Dalitz plot that only one $\mathbf{K}_\alpha$ contributes, one gets an estimate of g_1^2/g_0^2 from the observed strengths,

$$\frac{W_{\mathrm{QFA}}(np\to nn)}{W_{\mathrm{QFA}}(pp\to np)} \cong \frac{2g_1^2}{2g_0^2+g_1^2} = \frac{5.9}{64.8} \Longrightarrow \frac{g_1^2}{g_0^2} \cong 0.095 \tag{16}$$

or $g_1^2/g_0^2\simeq0.095$, much smaller than any entry in Table II obtained from the nucleon-nucleon pion production experiments. The qualitative result is not contradicted by the more accurate results presented in the next section.

III. NUMERICAL RESULTS

A few general remarks should be made before presenting in detail the numerical results of our calculations. (1) The rates in all cases are homogeneous of second degree in g_0, g_1 [Eqs. (10a)–(10c) and (13)]. Keeping g_0 fixed at values determined from relatively accurate measurement of the $p+p\to d+\pi^+$ cross section, the rates can be treated as functions of a single variable g_1/g_0. (2) The calculated rate $W^{1s}(n+d)$ and the sums of the calculated rates $W^{1s}(nnp\ \mathrm{FSI})+W^{1s}(nnp\ \mathrm{QFA})=W^{1s}(nnp)$ can be compared to measured $1s$ rates[15] directly without further assumptions. (3) The individual calculated FSI rates $W^{1s}(n+{}^1np_0)$ and $W^{1s}(p+{}^1nn_0)$ can be compared to data assuming the relative percentages of stopped pions yielding $n+d$ and nnp FSI states, respectively, are the same as for pure $1s$ absorption. (4) If it is further assumed that the spectrum of particles attributed to nnp QFA measured for stopped pions is reflective of the spectrum for $1s$ absorption alone, the calculated $1s$ differential absorption rate to nnp QFA can be compared to the Dalitz plot. (An analysis of the K x-ray yields[26] indicates that $87\pm6\%$ of the pion absorptions take place from s states in ^{3}He gas of the appropriate density.) (5) The rate (s^{-1}) of a process is, of course, proportional to the width (ev) connected with the same process. Throughout the remainder of this paper we distinguish the two by using the symbols W and Γ, respectively.

A. $1s$ absorption rates to $n+d$ and nnp FSI

The calculated $1s$ absorption rates leading to the nd, the $n^1(np)_0$, and $p^1(nn)_0$ final states, obtained from Eqs. (10a)–(10c), are to be found in Table III. The rates for values of g_1/g_0 compatible with the two-nucleon production data, taken from Table II, as well as for $g_1/g_0=0$ have been tabulated. The rates corresponding to the Yukawa form factor are more stable because the exponential form factor varies much more rapidly with the range a for a fixed momentum. For physical reasons the Yukawa is preferable, and all further remarks are addressed to that case.

The calculated partial rates for $W^{1s}(n+d)$ are compared to a recently measured experimental value. By measuring the branching ratio for absorption leading to nd in coincidence with K x rays, Backenstoss *et al.*[15] have obtained an absolute rate $W^{1s}(n+d)=0.58\pm0.10\times10^{16}$ s^{-1}. Their quoted result does not include the uncertainty

TABLE III. Calculated partial rates [Eqs. (10a), (10b), and (10c)] for absorption of $1s$ π^- leading to nd, $n^1(np)_0$, and $p^1(nn)_0$ final states. The rates are calculated for both signs of $x=\pm(g_1^2/g_0^2)^{1/2}$, where g_1^2 and g_0^2 are taken from Table II. Experimental values of the rates are to be found at the bottom of the table. All rates are in units of 10^{16} s^{-1}.

Range (fm)	Form factor	Hard-core function					Hulthen function		
		$W^{1s}(n+d)$			$W^{1s}(p+nn)$	$W^{1s}(n+nP)$	$W^{1s}(n+d)$		
		$x<0$	$x>0$	$x=0$			$x<0$	$x>0$	$x=0$
0.6	Exponential	0.31	1.14	0.34			0.27	1.00	0.36
0.6	Yukawa	0.34	1.25	0.41	0.057	0.39	0.24	0.90	0.33
1.0	Exponential	0.52	2.03	0.50			0.35	1.26	0.44
1.0	Yukawa	0.37	1.34	0.45	0.063	0.40	0.26	0.98	0.35
1.4	Exponential	0.84	1.98	0.67			0.40	1.49	0.50
1.4	Yukawa	0.41	1.51	0.47	0.068	0.40	0.28	1.03	0.36
1.8	Exponential	1.29	2.21	0.85			0.44	1.64	0.54
1.8	Yukawa	0.44	1.63	0.50	0.068	0.41	0.29	1.07	0.38
			$W^{1s}(n+d)=0.58\pm0.19$[a]				$W^{1s}(n+np)=0.42\pm0.11$[b]		
			$W^{1s}(n+d)=0.75\pm0.24$[c]				$W^{1s}(p+nn)=0.05\pm0.02$[b]		

[a]References 10 and 15.
[b]References 10, 13, and 15.
[c]References 9 and 15.

from $\Gamma_{tot}^{1s}=28\pm7$ eV,[10] but the additional 25% uncertainty has been included in the experimental result quoted in Table III. The deduced partial rate, obtained from the larger $\Gamma_{tot}=36\pm7$ eV,[9] is also tabulated, but all further comparisons are made with the smaller Γ_{tot}, since it is more compatible[27] with the branching ratio (radiative capture) per absorption. The calculated rates $W^{1s}(n+d)$ for $g_1/g_0>0$ are inconsistent with the data, while rates for $g_1/g_0<0$ are generally allowed. Treating g_1/g_0 as an adjustable parameter, agreement with the central experimental rate can be obtained for small positive g_1/g_0.

The calculated rates for the singlet *np* final state, depending only on g_0^2, is in good agreement with the "experimental" rate. The latter was obtained by scaling $W^{1s}(n+d)$ according to FSI partial rates, expressed as percentages listed in Table I. While some stopped pion events have significant pion *p*-state contributions, there is some evidence that the *nd* channel [and presumably, the $n\,^1(np)_0$] has little room left for *p* absorption.[15] From Table I,

$$W^{1s}[n+{}^1(np)_0]=(11.7/16.1)\times W^{1s}(n+d)$$
$$=(0.42\pm0.11)\times10^{16}\ \mathrm{s}^{-1} \quad (17a)$$

and

$$W^{1s}[p+{}^1(nn)_0]=(1.5/16.1)\times W^{1s}(n+d)$$
$$=(0.05\pm0.02)\times10^{16}\ \mathrm{s}^{-1}\ . \quad (17b)$$

The latter rate is in excellent agreement with the calculated $W^{1s}[p+{}^1(nn)_0]$ entered in Table III. However this is the only piece of ^{3}He data that can be well fit by fixing g_1 at the value derived from the π^0 production cross sections. Because of its small size, it is our opinion that the rate calculated for the process in question is the least reliable of all the calculated rates. The wave function of Eq. (9) neglects final-state coupling between $n+d$, $n+{}^1np_0$, and $p+{}^1nn_0$ channels, which exists physically at some level. Coupling will, presumably, have a small effect on the large rates, but a significant effect on the small rates.

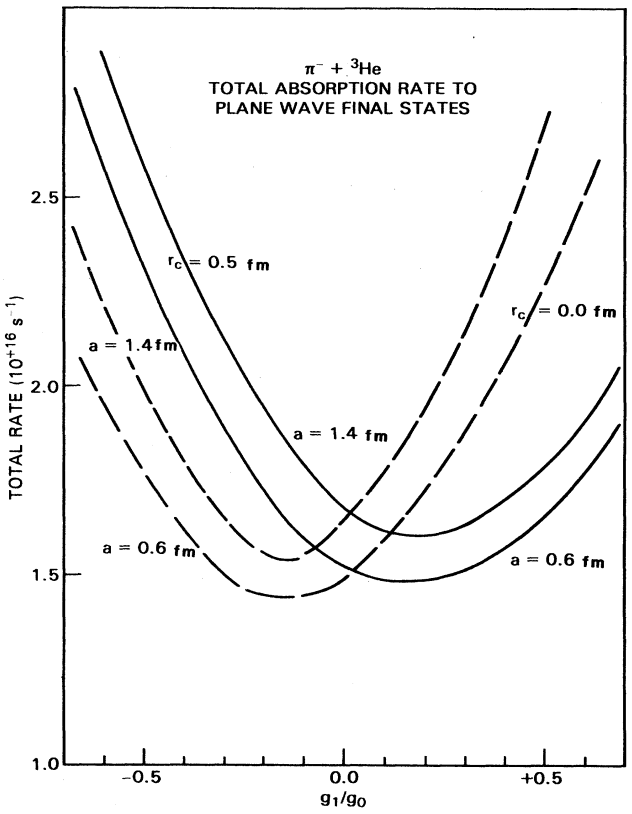

FIG. 1. The total 1*s* absorption rate for stopped pions in ^{3}He as a function of the ratio of the parameters describing absorption on singlet and triplet spin nucleon pairs. The curves were calculated according to Eq. (13), and are distinguished from each other by the type of nucleon-nucleon correlation, hard core ($r_c=0.5$ fm) or Hulthen ($r_c=0.0$ fm), and by the intermediate state pion range *a*. The values of g_0^2 used in this figure, and all subsequent ones, are taken from Table II of the text. No corrections to the pion Coulombic wave function resulting from strong interactions have been included in the rates.

B. Total 1*s* absorption rate to *nnp* FSA

The total rates for 1*s* quasifree pion absorption, approximated in our calculation by transitions to free-particle three-body states, have been calculated using Eq. (13) and are plotted vs g_1/g_0 in Fig. 1. Two different Yukawa form factors, $a=0.6$ and 1.4 fm, have been used with both the Hulthen and hard-core correlations. The $R_{1s}^2(0)=1.05$ correction has not been included.

C. Spectrum of *nnp* QFA nucleons following 1*s* absorption

The data to which the g_1/g_0 ratio is most sensitive are the contour lines of the Dalitz plot for the three-body final states. The axes of the plot are associated with the proton kinetic energy and the kinetic energy of the observed neutron. The calculated number density of events is proportional to the integrand of Eq. (13), which can be written as $d^2W^{1s}(nnp\ \mathrm{QFA})/dT_p\,dT_n$. We have compared our theoretical results to the data by calculating the relative rates along certain straight lines in the Dalitz plot. In the notation of Fig. 1, Ref. 13, the lines are *DB*, *FB*, and *EC*.

The line *DB* runs from the point *D* representing quasifree absorption on an *np* pair (spectator proton at rest) to point *B* representing quasifree absorption on the *pp* pair (spectator neutron at rest). Each experimental point plotted in Fig. 2 is the intersection of the line *DB* with a contour line. The curves were calculated for $a=1.4$ fm, $r_c=0.5$ fm, and g_1/g_0 values, which either (1) fit the two-nucleon production data or (2) yield the observed $W^{1s}(n+d)$ rate. The deep minima in all the curves at $T_p=30$ MeV are due to a zero in the integral factor in $\mathbf{K}_3$ [Eqs. (13) and (14)]. The rate scale along the ordinate applies solely to the theoretical curves since the experimental data, being a sum of absorptions from *ns* and *np* atomic states, cannot be interpreted as a simple rate. However, the shape of the curves for all *s* states should be the

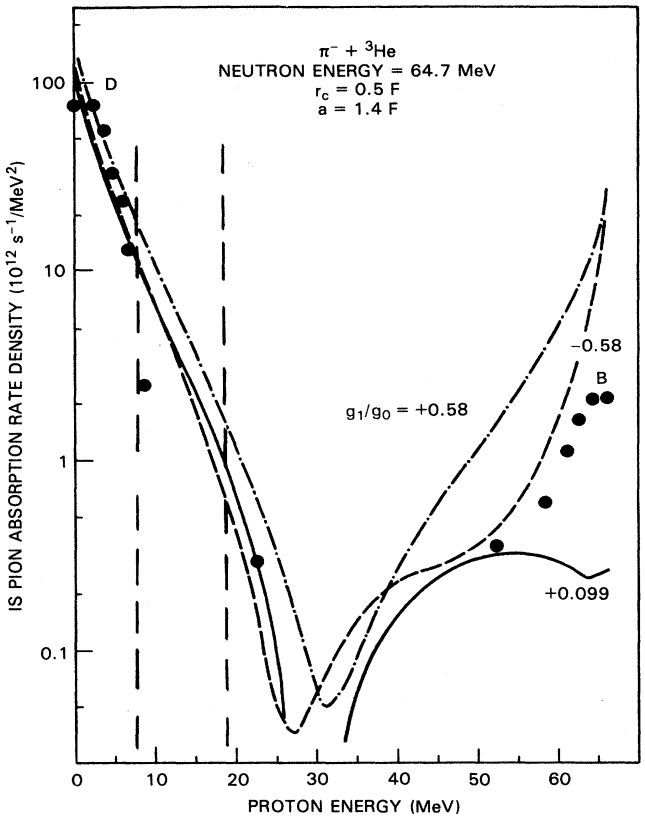

FIG. 2. Theoretical 1s absorption rate density in a Dalitz plot of three-body events as a function of T_p along a line of constant T_n. The point D corresponds to QFA on an np pair with the spectator proton at rest, while point B represents QFA on the pp pair with the neutron at rest. (The notation agrees with the experimental Dalitz plot of Ref. 13). The values $g_1/g_0 = \pm 0.58$ are determined by fitting the two-body production data and $g_1/g_0 = +0.099$ yields the experimental $\Gamma_{ab}^{1s}(nd)$. The normalization of the experimental points is arbitrary. The rate densities from the integrand of Eq. 13 include the factor 1.05 as a strong interaction correction. The range of proton energies within the vertical dotted lines corresponds to a region of the Dalitz plot, in which event rates could not be measured by virtue of the experimental setup. The single experimental point within this region was obtained by extrapolation of the corresponding contour line into the excluded region.

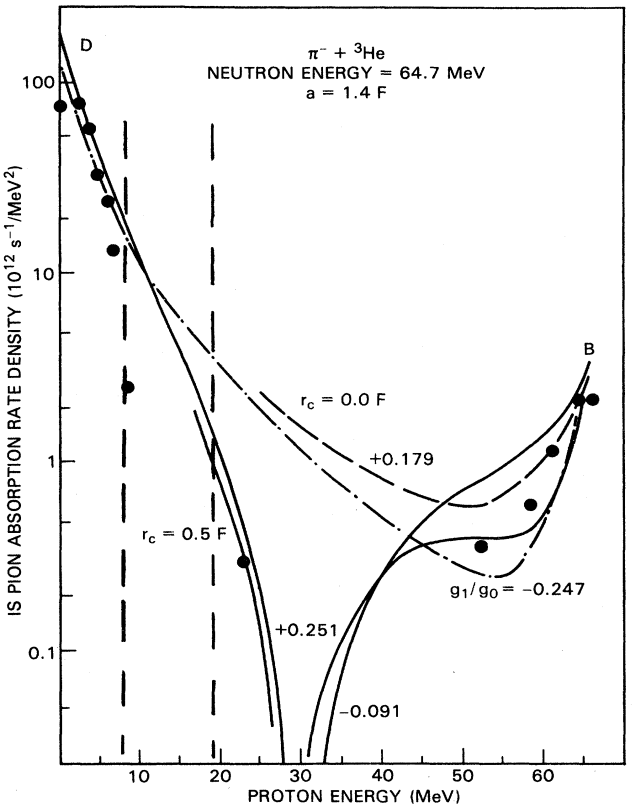

FIG. 3. Theoretical 1s absorption rate density along the same kinematic locus as in Fig. 2. The values of g_1/g_0 have been adjusted so that the theory yields the experimental ratio of strength at B compared to D. The rate densities are calculated for both hard-core ($r_c = 0.5$ fm) and Hulthen two-nucleon correlations.

same. An arbitrary normalization for the data points has been adopted which is the same in subsequent figures. No attempt to fold experimental resolution into the theoretical curves has been made. Note that the quasi-free absorption rates on a pp pair are overestimated by more than a factor of 10 by the g_1^2/g_0^2 values, which are derived from the two-body production data.

Figure 3 displays the rates along the same line DB for both the hard-core and Hulthen correlations, with g_1/g_0 adjusted to yield the experimental magnitude at point B. Note that there is no deep minimum for the Hulthen case and, in fact, the curve for this case is an order of magnitude higher than the observed rates midway between the points D and B. That the integral factor in $\mathbf{K}_3$ has the same sign at all points along the Hulthen curve is also manifested by the fact that for this correlation the curve for $g_1/g_0 < 0$ tracks the data at B satisfactorily, while with the hard-core correlation a positive ratio, $g_1/g_0 > 0$, is required for a good fit. The sign of the interference term $\mathbf{K}_1 \cdot \mathbf{K}_3$ at B determines the preferred sign of g_1/g_0.

The line FB connects the two points on the Dalitz plot that are the centers for QFA on pp pairs. The comparison of the calculated relative rates along the line with the experimental data, Fig. 4, does not yield much additional information. Again the g_1/g_0 values determined from the two-nucleon analysis lead to an overestimate at the pp QFA peaks. A positive g_1/g_0 for the hard-core correlation fits the falloff of the data at the extremities of the symmetric curve far better than a negative g_1/g_0. The calculated values of the rates are all too high in the center of the range of proton energies. In this region $\mathbf{K}_3$ dominates, which indicates that the hard-core correlation, as may be expected, overestimates the high momentum components of the spectator particle wave function.

The line EC connects the two points of the Dalitz plot that represent zero relative momentum for an np pair, the

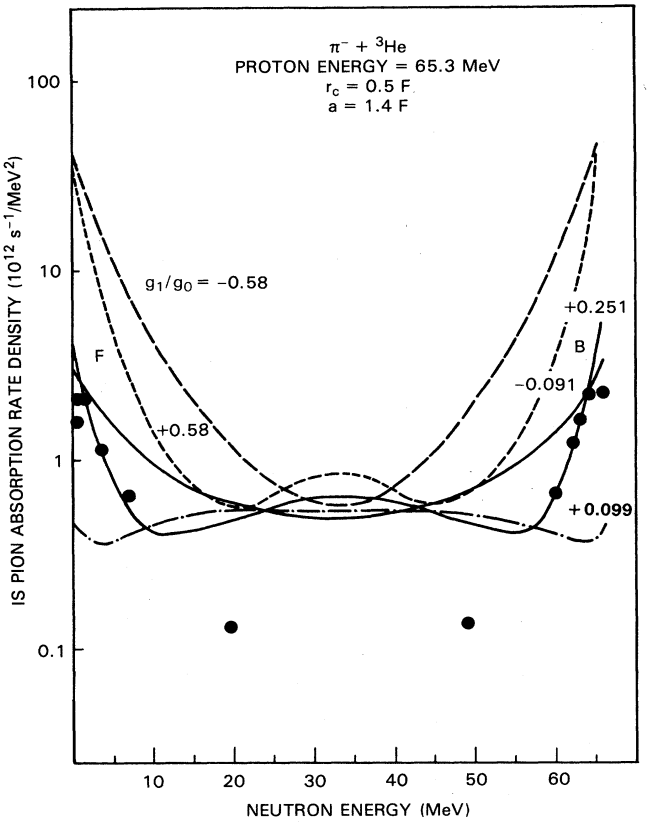

FIG. 4. Theoretical 1s pion absorption rate density plotted against T_n for fixed T_p. The points F and B correspond to QFA on pp pairs in ^{3}He, with the spectator neutron at rest. The curves are symmetric around the midpoint of the allowed neutron energy range because of the Pauli principle constraint, with respect to the neutron pair in the final state. The significance of each choice of g_1/g_0 is explained in the captions for Figs. 2 and 3. The same normalization of data points has been used.

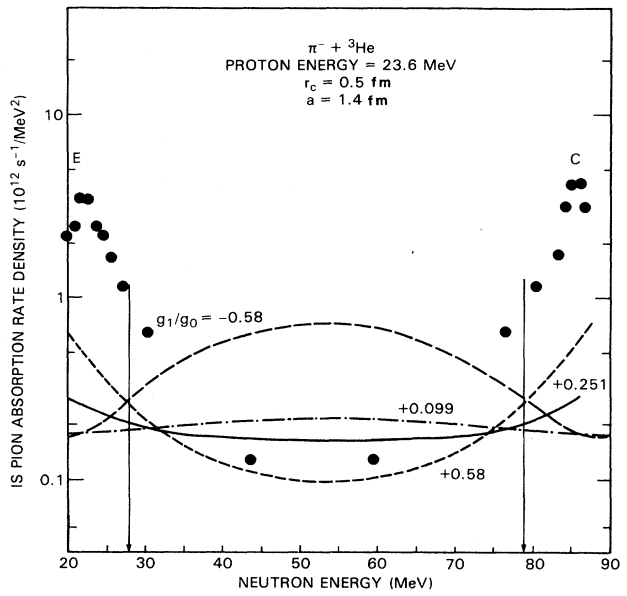

FIG. 5. Theoretical 1s pion absorption rate density plotted against T_n for $T_p=24.0$ MeV. The points E and C are the two np FSI points in the Dalitz plot, the points where $T_{np}=0$. The rates were calculated from Eq. (13) which approximates the final state by plane waves so no FSI is included in the calculation. The significance of each g_1/g_0 ratio is the same as in Figs. 2 and 3. The vertical arrows represent the position of the upper limit $P_f^{\max}$ on the integral over relative np momentum that appears in Eq. (10b).

centers of the nnp FSI regions. The approximate wave functions used for the rates in the FSI regions are in the three-body continuum. However, the comparison to experiment has already been made by integrating the calculated partial rates over the relative np momentum bounded by $0\leq p_f\leq p_f^{\max}=0.5$ fm^{-1} and comparing the result to the rates obtained by summing experimental events within the FSI regions (see bottom of Table III). To illustrate the importance of FSI the nnp QFA plane wave rates without FSI enhancement are shown in Fig. 5. The curves are given for $a=1.4$ fm, $r_c=0.5$ fm. As could be expected, all of them are at least an order of magnitude too small in the nnp FSI regions, but all except the curve for $g_1/g_0=-0.58$ fit the data in the middle, again an indication that g_1/g_0 is positive. The vertical lines show the limits along EC corresponding to the $p_f^{\max}=0.5$ fm^{-1} upper limit for the singlet deuteron strength in Eq. (10b).

D. Constraints on g_1/g_0 from the experimental ^{3}He data

The absolute experimental $W^{1s}(n+d)$ and $W^{1s}(nnp)$ rates have large uncertainties because they include the 25% uncertainty in $\Gamma_{\rm tot}^{1s}$. However, the ratio $\Gamma_{\rm ab}^{1s}(nd)/\Gamma_{\rm ab}^{1s}$ (three body), that has been determined in a branching ratio and K x-ray yield experiment,[15] is independent of $\Gamma_{\rm tot}^{1s}$. From this experiment one obtains the relationship

$$\Gamma_{\rm ab}^{1s}(nd)/\Gamma_{\rm ab}^{1s}\ (\text{three body})=0.31\pm0.07\ .$$

The theoretical ratios for the hard-core and Hulthen correlations are plotted in Figs. 6 and 7, respectively, as functions of g_1/g_0 (the g_0 dependence cancels). The singlet rates in Table III have been added to the QFA rates from Fig. 1 to get the theoretical $\Gamma_{\rm ab}^{1s}$ (three body). The experimental values and uncertainties are plotted as horizontal lines in the figures. Other limitations on g_1/g_0 are also represented on Figs. 6 and 7. The ranges of g_1/g_0 that are consistent with the observed partial absorption rates $W^{1s}(n+d)$ are delimited by vertical dotted lines that bracket the cross-hatched uncertainties. The solid vertical lines with the accompaning horizontal arrows show the ranges of g_1/g_0 that are acceptable in so far as the relative heights of the pp QFA and pn QFA peaks are concerned. The arrows are directed inwardly because it has been assumed that the singlet/triplet NN ratio for p-state pion absorption is of the order of 0.1,[28] as large or larger than the ratio for s-state absorption. The values of g_1/g_0 that are consistent with two-nucleon pion production are indicated on both Figs. 6 and 7, and are not consistent with most of the ^{3}He data in either case.

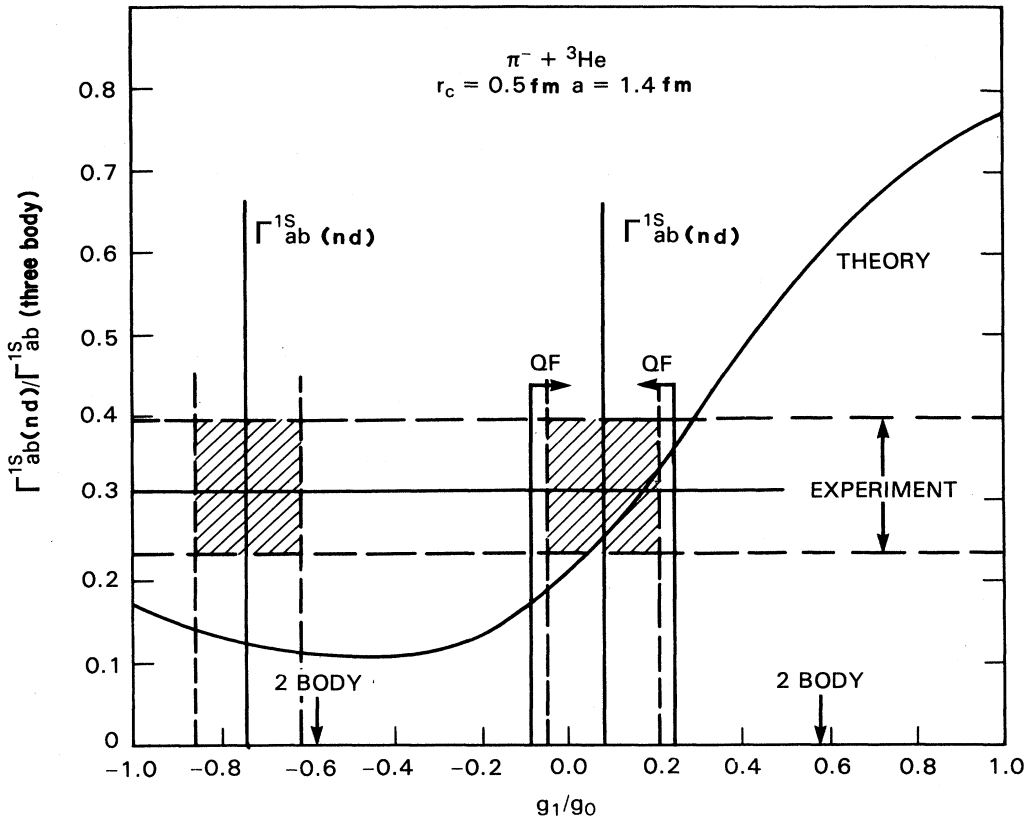

FIG. 6. The plotted curve is the theoretical ratio of the 1s absorption rate to two-body (nd) and three-body (nnp) final states. The three-body rate is the sum of the calculated rates for nnp QFA (Fig. 1) and the total rates to the nnp FSI regions of the Dalitz plot (Table III). The experimental ratio and the error limits[15] are shown by the horizontal solid and dashed lines, respectively. The vertical dashed lines show the limits on g_1/g_0 that correspond to the experimental limits on $\Gamma^{1s}_{ab}(nd)$. The vertical solid lines marked QF delineate the values of g_1/g_0, which yield theoretical ratios of absorption strength on pp relative to np pairs in agreement with experiment (see Fig. 3). The short vertical arrows show the g_1/g_0 values fixed by the pp production cross sections. The values of g_1/g_0 for which the solid curve passes through the cross-hatched area are those for which the agreement within error limits to all ^{3}He data is possible.

One concludes from these figures that when Hulthen nucleon-nucleon correlations are used no satisfactory value of the ratio g_1/g_0 can be found which allows a fit to all the three-body data. On the other hand, there is a range of acceptable values of g_1/g_0, $0.03 < g_1/g_0 < 0.21$, when the hard-core nucleon-nucleon correlations are included in the ^{3}He wave function.

IV. DISCUSSION

The absorption or production of low-energy pions interacting with S-state nucleon pairs occurs predominantly on $S=1$, $T=0$ nucleon pairs. The phenomenological two-nucleon t matrix describing $p+p \rightarrow d+\pi^+$ provides a satisfactory description of absorptions of stopped π^- on triplet np pairs in ^{3}He. In particular, the calculated partial rates for $\pi^- + {}^3\text{He} \rightarrow n + {}^1(np)_0$, proportional to the parameter g_0^2, and the QFA rate of π^- on np pairs in ^{3}He, depending primarily on g_0^2, are in good agreement with experiments.[13,15] The experimental partial 1s rate to nd can be accommodated by choosing g_1/g_0 values that are much smaller than the ones required to fit $p+p \rightarrow p+p+\pi^0$. Small positive values of g_1/g_0 are also consistent with the relative size of the Dalitz plot peaks[13] from the QFA of π^- on pp pairs. Our conclusion is that all the data associated with absorption of stopped pions in ^{3}He can be accounted for within the framework of a two-nucleon absorption model provided the nuclear ground state contains strong repulsive correlations, and the importance of absorption on singlet nucleon pairs is suppressed compared to that indicated by two-nucleon threshold pion production experiments. On the other hand, there is strong experimental evidence that a direct three-nucleon pion absorption process plays an important role for 120-MeV pions incident on ^{3}He.[29,30] The $3N$ mechanism was established through the observation of significant cross sections for those absorption events where final states are kinematically far from QFA or FSI regions. However, the authors of Ref. 29 state that if the same analysis is applied to the stopped pion-absorption data[13] a $3N$ absorption rate of less than 10% of the total absorption rate can be derived, which is not in disagree-

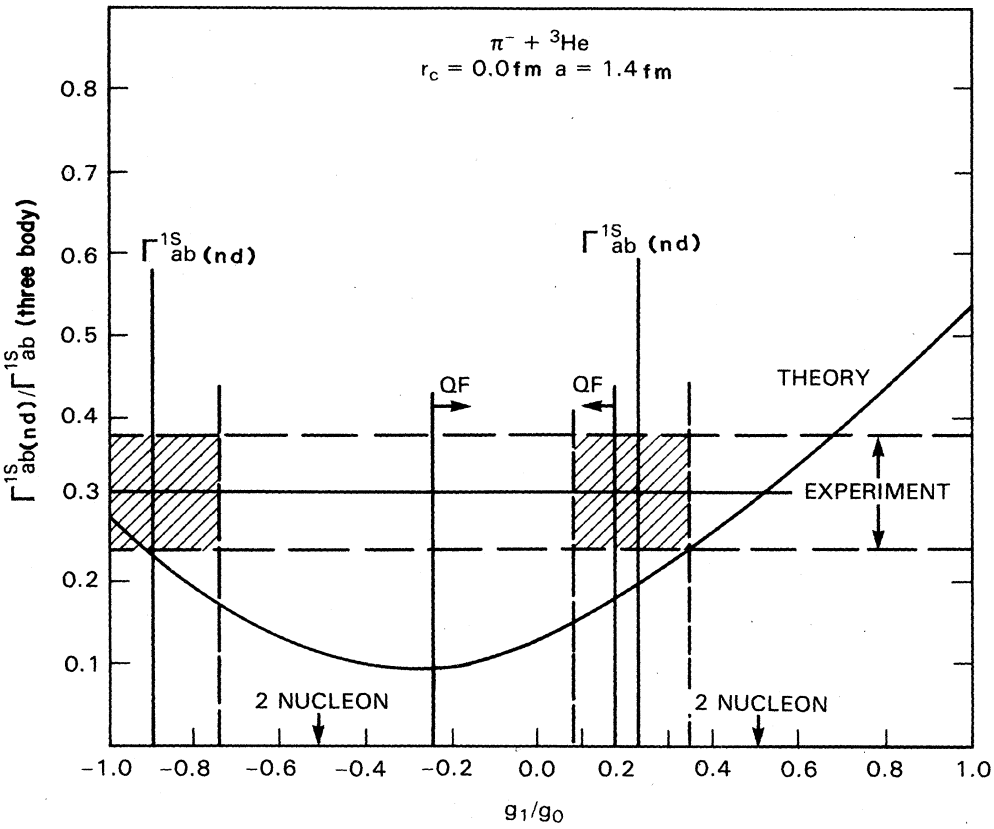

FIG. 7. The same as Fig. 6 except all calculations were carried out with the Hulthen nucleon-nucleon correlation instead of the hard core. No value of g_1/g_0 can be found which is consistent with all ^{3}He data.

ment with our results.

There are at least two reasons that separately or in combination may account for the inconsistency of the two-nucleon model in the spin-singlet pair case. These are (1) confusion of the true signal for π^0 production with another process, *pp* bremsstrahlung, in the production experiments, and (2) a significant contribution of the one-nucleon absorption amplitude to the process which may interfere differently with the two-nucleon amplitude in the two- and three-nucleon systems, respectively.

The two references for π^0 production from $p+p \rightarrow p+p+\pi^0$ cited in this paper, Refs. 21 and 22, were both single arm experiments, that is if only one decay gamma was observed. The total cross sections obtained are of the order of a few μb. For certain geometries *p-p* bremsstrahlung differential cross sections[31] amount to as much as $10\mu b/\text{sr}^2$ for $E_p = 200$ MeV. It is conceivable that many of the gamma counts for proton energies just above the π^0 threshold originated from the *p-p* bremsstrahlung process. In any event it would be worthwhile to make modern measurements of the fundamental production cross section.

Koltun and Reitan[16] calculated the nucleon-nucleon pion production cross sections near threshold assuming the process is due to a sum of one- and two-nucleon amplitudes. The input to the one-body amplitude is the pion-nucleon coupling constant and the two-nucleon production amplitude requires, in addition, the two pion-nucleon scattering lengths, with values fixed by experiment. The authors found that the small single nucleon amplitude played no role in the production or absorption of low-energy pions on triplet spin nucleon-nucleon pairs. However, because of the small size of the isoscalar pion-nucleon scattering length the two-nucleon production amplitude for singlet pairs is strongly suppressed, so that the one-nucleon amplitude becomes comparable. Somewhat in support of (1) they calculated a $p+p \rightarrow p+p+\pi^0$ cross section about 40% lower than measured (still within the experimental error bars). The relative two-nucleon wave function for a spin-singlet pair inside ^{3}He certainly differs from the low-energy *pp* two-nucleon wave function. It is plausible that the expectation value of the sum of the one- and two-nucleon absorption amplitudes results from a delicate balance of the two terms so that singlet absorption in ^{3}He is suppressed compared to that expected from π^0 production experiments.

In our model, the rapid falloff of the event rate along line *DB* in the Dalitz plot (see Figs. 2 and 3) as well as the virtually complete absence of events near its center are the direct result of short-range nucleon-nucleon correlations in the ^{3}He ground state. At the QFA point the pair of emitted nucleons have relative momentum $p \simeq (M_\mu)^{1/2} = 1.83$ fm^{-1} so that ground-state nucleon-nucleon correlations at distances of the order of 0.54 fm

can be probed. In the two-nucleon system ($p+p \rightarrow d+\pi^+$) the (initial) pair momentum is fixed near this value, whereas, absorption on a pair in ^{3}He can be observed for a wide range of $p < 1.83$ fm^{-1}. The Fourier transform of the ground-state wave function $u(\mathbf{p},\mathbf{q})$ changes sign as a function of p over this range, Eqs. (8) and (A1), so that the integral $\mathbf{K}_3$ [Eq. (14)] can likewise change sign as a function of the observed final momenta. The caveat must be made that this result has been derived using plane waves to represent the $^3P_1$ "high-energy" nucleons in both the production and QFA amplitudes. The behavior of both T-matrix elements when the nucleon pair is represented by a realistic $^3P_1$ scattering state is being investigated.

The complete understanding of absorption of low-energy pions in ^{3}He also awaits a better knowledge of the effect of p-wave absorptions. Such knowledge will come from the calculation of the two- and three-body spectra following p-wave absorption and/or the production of separate experimental Dalitz plots for s-wave and p-wave absorptions.

APPENDIX

A. Deuteron momentum space wave function

In configuration space, the hard-core deuteron function $\Phi_d(\mathbf{r})$ is given by formula (5a). In momentum space the hard-core deuteron function, obtained by taking Fourier transform of the function in (5a), becomes

$$\Phi_d(\mathbf{p}) = \sqrt{2/\pi} N \beta_d [(2\alpha_d+\beta_d)/(\alpha_d^2+p^2) \times \{[\cos(pr_c)+(\alpha_d^2+\alpha_d\beta_d-p^2)\sin(pr_c)/(2\alpha_d+\beta_d)p]/[(\alpha_d+\beta_d)^2+p^2]\}, \quad \text{(A1)}$$

where N is the normalization constant. The factor inside the curly brackets is the form factor $g_d(p)$, determined by the nonasymptotic behavior of the deuteron wave function.

B. Singlet deuteron momentum space wave function

In configuration space the singlet deuteron function $\Phi_{p_f}(\mathbf{r})$ is given by formula (5b). Again taking Fourier transform of that function we obtain for the singlet deuteron function in momentum space the following formula:

$$\begin{aligned}\Phi^-_{p_f}(\mathbf{p}) = \{[2e^{-i\delta}]/[(2\pi)^2 p p_f]\} \\ \times \big(\{\cos[(p-p_f)(R+r_c)/2-\delta]\sin[(p-p_f)(R-r_c)/2]/(p-p_f)\} \\ -\{\cos[(p+p_f)(R+r_c)/2+\delta]\sin[(p+p_f)(R-r_c)/2]/(p+p_f)\} \\ +[a/(\beta_s^2+p^2)]\{e^{-\beta_s R}[\beta_s\sin(pR)+p\cos(pR)] \\ -e^{-\beta_s r_c}[\beta_s\sin(pr_c)+p\cos(pr_c)]\}\big),\end{aligned} \quad \text{(A2)}$$

where

$$a = e^{-\beta_s r_c}\sin(p_f r_c+\delta)$$

and R is the cutoff radius.

[1] D. A. Ashery and J. P. Schiffer, Annu. Rev. Nucl. Part. Sci. **36**, 207 (1986).
[2] K. A. Brueckner, R. Serber, and K. M. Watson, Phys. Rev. **84**, 258 (1951).
[3] S. G. Eckstein, Phys. Rev. **129**, 413 (1963).
[4] P. P. Divakaran, Phys. Rev. **139**, B387 (1965).
[5] A. Figureau and M. Ericson, Nucl. Phys. **B10**, 349 (1969).
[6] C. Pajares and R. Pascual, Nucl. Phys. **335**, 631 (1971).
[7] A. C. Phillips and F. Roig, Nucl. Phys. **B60**, 93 (1973).
[8] O. A. Zaimidoraga *et al.*, Zh. Eksp. Teor. Fiz. **5**, 1646 (1966) [Sov. Phys.-JETP **24**, 1111 (1967)].
[9] G. R. Mason *et al.*, Nucl. Phys. **A340**, 240 (1980).
[10] I. Schwanner *et al.*, Nucl. Phys. **A412**, 253 (1984).
[11] P. Truoel *et al.*, Phys. Rev. Lett. **32**, 1268 (1974).
[12] J. McCarthy *et al.*, Phys. Rev. C **11**, 266 (1975).
[13] I. D. Gotta *et al.*, Phys. Lett. **112B**, 129 (1982).
[14] A. V. Bannikov *et al.*, Nucl. Phys. **A403**, 515 (1983).
[15] G. Backenstoss *et al.*, Nucl. Phys. **A448**, 567 (1986).
[16] D. C. Koltun and A. Reitan, Phys. Rev. **141**, 1413 (1966).
[17] B. Goplen, W. R. Gibbs, and E. C. Lomon, Phys. Rev. Lett. **32**, 1012 (1974).
[18] K. Shimizu and Amand Faessler, Nucl. Phys. **A306**, 311 (1978); K. Shimizu, A. Faessler, and H. Muether, *ibid.* **A343**, 468 (1980).
[19] A. H. Rosenfeld, Phys. Rev. **96**, 139 (1954).
[20] David G. Long, Morton M. Sternheim, and Richard R. Silbar, Phys. Rev. C **26**, 586 (1982).
[21] A. F. Dunaitsev and Y. D. Prokoshkin, J. Eksp. Teor. Phys. **36**, 1656 (1959) [Soviet Phys.—JETP **9**, 1179 (1959)].
[22] R. A. Stallwood, R. B. Sutton, T. H. Fields, J. G. Fox, and J. A. Kane, Phys. Rev. **109**, 1716 (1958).
[23] H. Pierre Noyes, Annu. Rev. Nucl. Sci. **22**, 465 (1972).

[24]Carl Werntz and H. S. Valk, Phys. Rev. Lett. **54**, 3321 (1985).
[25]I. M. Barbour and A. C. Phillips, Phys. Rev. C **1**, 165 (1970).
[26]Rolf Landua, Ph.D. thesis, Johannes Gutenberg University, Mainz, 1980.
[27]Carl Werntz and H. S. Valk, Phys. Rev. C **37**, 724 (1988).
[28]Richard R. Silbar and E. Piasetzky, Phys. Rev. C **29**, 1116 (1984).
[29]G. Backenstoss *et al.*, Phys. Rev. Lett. **55**, 2782 (1985).
[30]H. J. Weyer, Helv. Phys. Acta **60**, 667 (1987).
[31]Ebbe M. Nyman, Phys. Rev. **170**, 1628 (1968).